Quantum interference on the *kagomé* lattice

Yeong-Lieh Lin and Franco Nori

Department of Physics, The University of Michigan, Ann Arbor, Michigan 48109-1120

(Received 22 June 1994; revised manuscript received 8 August 1994)

We study quantum interference effects due to electron motion on the *kagomé* lattice in a perpendicular magnetic field. These effects arise from the interference between phase factors associated with different electron closed paths. From these we compute, analytically and numerically, the superconducting-normal phase boundary for *kagomé* superconducting wire networks and Josephson junction arrays. We use an analytical approach to analyze the relationship between the interference and the complex structure present in the phase boundary, including the origin of the overall and fine structure. Our results are obtained by exactly summing over $\sim 10^{21}$ closed paths, each one weighted by its corresponding phase factor representing the net flux enclosed by each path. We expect our computed mean-field phase diagrams to compare well with several proposed experiments.

I. INTRODUCTION

Interest in *kagomé* structures has been fueled by several recent developments. The first one refers to a central question in magnetism: the $T = 0$ order of the two-dimensional (2D) nearest-neighbor-coupled Heisenberg antiferromagnet. The *kagomé* lattice seems to be the first 2D spin-1/2 model with vanishing farther-neighbor interactions which appears to have a disordered ground state.[1] Second, measurements of the heat capacity of ^{3}He absorbed on graphite at millikelvin temperatures have been recently interpreted using a *kagomé* lattice structure.[2] Third, measurements on the layered oxide $SrCr_{8-x}Ga_{4+x}O_{19}$, with *kagomé*-like layers, are currently attracting considerable attention.[3]

The connection between the *ideal kagomé* network and the *real* structures mentioned above (e.g., ^{3}He absorbed on graphite and $SrCr_{8-x}Ga_{4+x}O_{19}$) is somewhat unclear because of the very important effects of disorder, impurities, three dimensionality, etc., present in those materials. On the other hand, superconducting networks, made with electron-beam lithography, offer the possibility of experimentally studying *nearly perfect kagomé* structures. When immersed in an externally applied magnetic field, superconducting networks[4] made of thin wires, proximity-effect junctions, and tunnel junctions exhibit complex and interesting forms of phase diagrams (i.e., the resistive transition temperature as a function of the magnetic field).

The goals of this paper are to analytically study quantum interference effects of very many ($\sim 10^{21}$) electron closed paths on a *kagomé* lattice in a transverse magnetic field B, and from these to theoretically predict a measurable quantity, the field-dependent superconducting-normal phase boundary $T_c(B)$, for superconducting *kagomé* networks. The study of quantum interference effects is also important for other physical processes. For instance, von Delft and Henley[5] have recently investigated destructive quantum interference between different paths that connect the same initial and final configura-

tions in order to study spin tunneling events on a *kagomé* lattice.

II. SUMMARY OF RESULTS

The principal results presented in this paper are the following: (1) an analytic study of electron quantum interference effects from sums over magnetic phase factors on closed paths, (2) a very efficient computation of these "discrete path integrals" in closed-form expressions, and (3) from the latter, the derivation of $T_c(B)$. The lattice path integrals obtained here are "many-loop" generalizations of the standard "one-loop" Aharonov-Bohm-type argument (where the electron wave function picks up a phase factor $e^{i\Phi}$ each time it goes around a closed loop enclosing a net flux Φ).

The calculation of lattice path integrals will enable us to obtain the phase boundaries[6] through an iterative approach. The spirit of the approach follows Feynman's programme: to derive physical quantities in terms of "sums over paths." This method is considerably different from the standard ones for computing $T_c(B)$ (e.g., numerically diagonalizing the Ginzburg-Landau equations for large and/or irregular structures). We will examine these issues in more detail below.

III. QUANTUM INTERFERENCE FROM SUMS OVER PATHS

A. Physical interpretation

The physics of $T_c(B)$ is determined by the electronic *kinetic* energy because the applied field induces a diamagnetic current in the superconductor.[4] This current (i.e., a velocity) determines the kinetic energy of the system. In other words, the kinetic energy can be written in terms of the temperature as

$$-\frac{\hbar^2}{2m^*}\nabla^2 \sim -\frac{\hbar^2}{2m^*\xi(T)^2} \sim T_c(B) - T_c(0),$$

where, for any superconductor, m^* is twice the electron mass, and $\xi(T) = \xi(0)/[1 - T_c(B)/T_c(0)]^{1/2}$ is the temperature-dependent coherence length. We thus consider the electronic kinetic energy

$$H = \sum_{\langle ij \rangle} c_i^\dagger c_j \exp(iA_{ij}), \tag{1}$$

on a discrete *kagomé* lattice in a magnetic field, where $A_{ij} = \int_i^j \mathbf{A} \cdot d\mathbf{l}$ is the line integral of the vector potential along the bond from i to j. Throughout this paper, we set equal to one the constant factor in A_{ij}, namely, 2π divided by the flux quantum $hc/2e$.

The lattice path integral (or moment) of order l, summarizing the contribution to the electron kinetic energy of *all* paths of l steps, is defined as

$$m_l \equiv \langle \psi_1 | H^l | \psi_1 \rangle, \tag{2}$$

where $|\psi_1\rangle$ denotes a localized one-site electron state. Let us examine more closely the physical meaning of m_l. The Hamiltonian H is applied l times to the initial state $|\psi_1\rangle$, resulting in the new state $H^l|\psi_1\rangle$ located at the end of the path traversing l lattice bonds. Because of the presence of a magnetic field, a factor $e^{iA_{ij}}$ is acquired by an electron when hopping through two adjacent sites i and j.

The above expectation value m_l is nonzero only when the path ends at the starting site. The geometric significance of m_l thus becomes clear: It is *the sum of the*
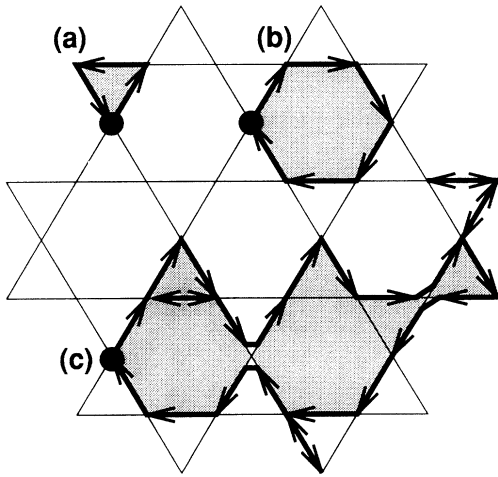

FIG. 1. Several examples of closed paths on a *kagomé* lattice and their respective phase factor contributions to the lattice path integrals. (a) Traversing counterclockwise a three-step path on an elementary triangular cell contributes a term $e^{i\phi}$ to m_3, (b) a six-step clockwise walk on an elementary hexagonal loop contributes a term $e^{-6i\phi}$ to m_6, and (c) a closed path of 26 steps with several links retraced. Its phase factor is $e^{-16i\phi}$. The solid dots denote the starting (and ending) sites and the arrows specify the hopping directions on bonds.
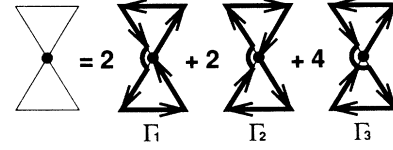

FIG. 2. An "hourglass" loop made of two triangles can be traversed in eight different ways, contributing three different phase factors to m_6. On the right-hand side, there are three possible different paths: Γ_1, Γ_2, and Γ_3. Path Γ_1 (Γ_2) contributes $e^{i\phi+i\phi} = e^{2i\phi}$ ($e^{-i\phi-i\phi} = e^{-2i\phi}$) to m_6. In path Γ_3 the phases cancel and the contribution of this path to m_6 is $e^{i\phi-i\phi} = 1$. The coefficients in front of the Γ's are the number of paths with the same phase factor.

contributions from all closed paths of l steps starting and ending at the same site, each with a phase factor of $e^{i\Phi_P}$ where Φ_P is the *net* flux enclosed by the closed path P, namely,

$$m_l = \sum_{\text{All closed paths}} e^{i\Phi_P}. \tag{3}$$

Here, quantum interference arises because the phase factors of different closed paths, including those from all kinds of distinct loops and separate contributions from the same loop, interfere with each other. Sometimes, the phases corresponding to subloops of a main path cancel.

Several examples of different paths on a *kagomé* lattice and their respective contributions to the lattice path integrals are illustrated in Fig. 1. Figure 2 shows three different paths traveling through the same loop and their separate phase factor contributions to m_6. It will be seen below that the phase factors describe, in a gauge-invariant way, the electron interference effects, due to the presence of a magnetic field, on the transition temperature, and they are the source of the rich structure present in the phase diagram.

B. Analytical calculations

We have worked out a considerable number of lattice path integrals (up to the 38th order) for the *kagomé* lattice in a uniform magnetic field. The first five moments can be easily computed by hand, while the higher-order moments can be most conveniently obtained by using recursion relations and symbolic manipulation programs. We have manually computed moments for the first 12 orders. The correctness of the calculated moments is assured by the consistency of the results obtained by hand and by computer. The details of the computational techniques used to compute high-order moments will be presented elsewhere.

It is instructive to explain how the first seven lattice path integrals are obtained. This will also clarify their physical meaning. Let ϕ be the flux through an *elementary* triangular cell in the *kagomé* lattice. Since there is no path of one step for returning an electron to its initial site, m_1 is always equal to zero. There are four closed

paths of two steps each [retracing each other on one bond ($\cdot\leftrightarrow$), where the $\cdot$ indicates the initial site]; thus

$$m_2 = 4 \cdot\leftrightarrow = 4\,e^{i0\phi} = 4 = z,$$

where z is the coordination number of the lattice.

There are four three-step closed paths enclosing a triangular cell [two counterclockwise ($\cdot\overset{\leftarrow}{\triangledown}$), like the one shown in Fig. 1(a), and two clockwise ($\cdot\overset{\rightarrow}{\triangledown}$)]. Thus

$$m_3 = 2 \cdot\overset{\leftarrow}{\triangledown} +2 \cdot\overset{\rightarrow}{\triangledown} = 2e^{i\phi} + 2e^{-i\phi} = 4\cos\phi.$$

There are 28 closed paths of four steps each: four retracing twice on one bond ($\cdot\overset{\leftrightarrow}{\leftrightarrow}$), 12 starting from a site connecting two adjacent bonds and retracing once on each bond ($\leftrightarrow\cdot\leftrightarrow$), and 12 moving two bonds away and then two bonds back to the original site ($\cdot\overset{\leftarrow\leftarrow}{\rightarrow\rightarrow}$). Since all of them enclose no area (i.e., no flux), then

$$m_4 = 4 \cdot\overset{\leftrightarrow}{\leftrightarrow} + 12 \leftrightarrow\cdot\leftrightarrow + 12 \cdot\overset{\leftarrow\leftarrow}{\rightarrow\rightarrow} = 28.$$

There are 60 closed paths (30 counterclockwise and 30 clockwise) with five steps each. Three of these steps enclose a triangular cell while the other two steps retrace each other (e.g., $\cdot\overset{\leftarrow}{\triangledown}\leftrightarrow$, $\cdot\overset{\rightarrow}{\triangledown}\leftrightarrow$, $\cdot\leftrightarrow\overset{\leftarrow}{\triangledown}$, $\cdot\leftrightarrow\overset{\rightarrow}{\triangledown}$, $\overset{\leftarrow}{\triangledown}\cdot\leftrightarrow$, and $\overset{\rightarrow}{\triangledown}\cdot\leftrightarrow$). Thus

$$m_5 = 30\,e^{i\phi} + 30\,e^{-i\phi} = 60\cos\phi.$$

Among the six-step closed paths, four of them enclose an elementary hexagonal cell [like the one shown in Fig. 1(b)], four paths go twice around the same triangle, 12 "hourglass" paths ($\bowtie$) surround two triangular cells (six enclosing 2ϕ and six enclosing -2ϕ), and 244 paths enclose no *net* flux. It follows then that

$$m_6 = 244 + 16\cos 2\phi + 4\cos 6\phi.$$

Among the seven-step closed paths, 28 of them enclosing adjacent triangular and hexagonal cells (14 counterclockwise and 14 clockwise) contribute $14e^{7i\phi}+14e^{-7i\phi} = 28\cos 7\phi$ to m_7. Since a triangular elementary cell can be traversed in 756 different ways, with four steps out of seven enclosing no area, it follows that

$$m_7 = 756\cos\phi + 28\cos 7\phi.$$

Below we present the results for m_8–m_{15}, while $m_{16} - m_{20}$ are listed in the Appendix and m_{21}–m_{38} will not be presented. They are

$$m_8 = 2412 + 416\cos 2\phi + 96\cos 6\phi + 80\cos 8\phi,$$

$$m_9 = 9216\cos\phi + 76\cos 3\phi + 36\cos 5\phi$$
$$+756\cos 7\phi + 120\cos 9\phi,$$

$$m_{10} = 25804 + 7560\cos 2\phi + 1860\cos 6\phi$$
$$+2480\cos 8\phi + 100\cos 10\phi + 20\cos 14\phi,$$

$$m_{11} = 112420\cos\phi + 2816\cos 3\phi + 1276\cos 5\phi$$
$$+14608\cos 7\phi + 4400\cos 9\phi + 44\cos 11\phi$$
$$+44\cos 13\phi + 176\cos 15\phi,$$

$$m_{12} = 290956 + 1119680\cos 2\phi + 656\cos 4\phi$$
$$+33120\cos 6\phi + 51984\cos 8\phi + 4560\cos 10\phi$$
$$+36\cos 12\phi + 1104\cos 14\phi + 672\cos 16\phi$$
$$+16\cos 22\phi,$$

$$m_{13} = 1385436\cos\phi + 66872\cos 3\phi + 30680\cos 5\phi$$
$$+248872\cos 7\phi + 104364\cos 9\phi + 2756\cos 11\phi$$
$$+2184\cos 13\phi + 8372\cos 15\phi + 1456\cos 17\phi$$
$$+52\cos 21\phi + 156\cos 23\phi,$$

$$m_{14} = 3405448 + 1774248\cos 2\phi + 31284\cos 4\phi$$
$$+559160\cos 6\phi + 929320\cos 8\phi + 127876\cos 10\phi$$
$$+2632\cos 12\phi + 35532\cos 14\phi + 32256\cos 16\phi$$
$$+1960\cos 18\phi + 56\cos 20\phi + 1260\cos 22\phi$$
$$+672\cos 24\phi + 28\cos 30\phi,$$

$$m_{15} = 17292440\cos\phi + 1307960\cos 3\phi + 627624\cos 5\phi$$
$$+3985380\cos 7\phi + 2047920\cos 9\phi + 97860\cos 11\phi$$
$$+68340\cos 13\phi + 246500\cos 15\phi + 74760\cos 17\phi$$
$$+1700\cos 19\phi + 3420\cos 21\phi + 10140\cos 23\phi$$
$$+1680\cos 25\phi + 120\cos 29\phi + 300\cos 31\phi.$$

Note that the even (odd) moments depend only on the even (odd) harmonics of the flux. These moments are obtained by summing an enormous number (10^{21}) of closed paths, each one weighted by its corresponding phase factor representing the net flux enclosed by the path.

These moments, and the m_{21}–m_{38} not shown, will be used in Sec. IV to obtain superconducting-normal phase boundary for the *kagomé* network.

C. Differences between our approach and the traditional moments and Lanczos methods

In electronic structure calculations there is a method to compute the density of states called the moments method. This is similar to our approach in the sense that both compute moments. However, also in statistical analysis moments are often used. Moments are simply a concept of wide applicability to a large number of dissimilar problems. For instance, the half-width half-maximum of a probability distribution can be expressed in terms of its second moment; the center of mass of a distribution can be expressed in terms of its first moment and the skewness or degree of asymmetry in terms of its third moment. Any mathematical function (e.g., probability distribution, Raman line shape, or any other function) can always be expressed in terms of an expansion using an infinite number of moments, although typically the first ten or so moments provide an excellent approximation to most functions. In our system, we have analytically computed moments to extremely high order (the first 38 moments).

We list several important differences between the standard "moments method" and our problem. The typical use of the moments method (i) focuses on the computation of electronic density of states (instead of superconducting T_c's), (ii) is totally *numerical* (instead of mostly analytical), (iii) is done at zero magnetic field (instead of

obtaining expressions with an explicit field dependence), (iv) does not focus on the explicit computation of path integrals, and (v) does not study the physical effects of quantum interference (which is at the heart of our calculation and physical interpretation).

In conclusion, the traditional use of the moments method in condensed matter is significantly different from the approach and problem studied here.

Another way to diagonalize Hamiltonians is called the Lanczos method. This method directly obtains the tridiagonal form, *without* computing the moments, and thus differs in a significant way from the approach used here (where the explicit computation of the moments is one of our goals, since they can be used for other electronic property calculations). Furthermore, it is not convenient to use standard Lanczos method in our particular problem because it is extremely difficult to directly derive the parameters and the states of the iterative tridiagonalization procedure. This is so because of the presence of the magnetic field. On the other hand, the moments method provides standard procedures to diagonalize a matrix *after* the moments are computed.

Our approach has features in common with the Lanczos method and features in common with the moments method (e.g., the computation of the moments, which is absent in the canonical Lanczos technique). More importantly, the five differences listed above [(i)–(v)] make our approach to this problem quite different to the standard (purely numerical) implementations of both the Lanczos and moments methods.

IV. *KAGOMÉ* SUPERCONDUCTING NETWORKS AND JOSEPHSON JUNCTION ARRAYS

The complex structure in $T_c(B)$ is essentially a result of quantum interference effects due to the electron kinetic energy and the multiconnectedness of the networks in a magnetic field. The magnetic fluxes through the elementary cells are useful parameters to characterize the interference effect. At zero magnetic field, the quantum interference effect is absent, and therefore the resistive transition temperature should have a peak.

Mean-field theory[4,6,7] is very effective in providing a quantitative description of the phase diagrams. For wire networks, the mean-field expression is given by the Ginzburg-Landau equation expressed in terms of the order parameters at the nodes. For a junction array, one has a set of self-consistent equations[7] for the thermally averaged pair wavefunctions of the grains. Such equations are linearized near the transition point, and the highest temperature (i.e., top eigenvalue) at which a nontrivial solution first appears is identified as the transition temperature. This can be seen because the kinetic energy of the system can be written in terms of the temperature as $-\hbar^2/[2m^*\xi(T)^2] \sim T_c(B) - T_c(0)$. Therefore, one is left to find the top spectral edge of an eigenvalue problem.[4,6,7] In summary, these equations can be mapped into a tight-binding Schrödinger problem for an electron hopping on a lattice immersed in a magnetic field and $T_c(B)$ is determined by the kinetic energy of the electrons (i.e., by the Hamiltonian H).

Now we are going to find the top spectral edge, which is proportional to the transition temperature. The best strategy for deriving eigenvalues and eigenvectors of symmetric matrices is to first reduce the matrix to some simple form, which is typically tridiagonal. All methods employed today (almost exclusively numerical, and not analytical as done here) are based on modifications of the Jacobi method. The latter has been in widespread use a long time before the Lanczos and moments methods were developed.

We choose a normalized initial electron state $|\psi_1\rangle$, which is strongly localized at one site, and perform the following expansion:

$$H|\psi_n\rangle = \gamma_n|\psi_{n-1}\rangle + \beta_n|\psi_n\rangle + \gamma_{n+1}|\psi_{n+1}\rangle, \qquad (4)$$

with the condition $|\psi_0\rangle \equiv 0$. The H matrix in the basis $|\psi_n\rangle$ is obviously in a real tridiagonal form. The expansion is useful because finite truncations give good approximations to the quantity we desire, i.e., the top spectral edge.

Each new state in this method expands outward by one more step from the site where the starting state is located. Thus an nth-order truncation can cover a region of radius n on the network.[6] Furthermore, the parameters in the truncated Hamiltonian are gauge-invariant quantities.

The nonzero matrix elements β's and γ's can be exactly expressed in terms of the moments of the Hamiltonian by using the following novel and systematic procedure. First, define the auxiliary matrix M with the first row elements given by $M_{0,l} \equiv m_l$. The other rows are evaluated by using only one immediate predecessor row through

$$M_{n,l} = \frac{M_{n-1,l+2} - M_{n-1,1} M_{n-1,l+1}}{M_{n-1,2} - M_{n-1,1}^2} - \sum_{k=0}^{l-1} M_{n,k} M_{n-1,l-k}, \qquad (5)$$

where n and $l \geq 1$. The β_n's and γ_n's are obtained from the elements of the second and third columns as

$$\beta_n = M_{n-1,1} \qquad (6)$$

and

$$\gamma_n = \sqrt{M_{n-1,2} - M_{n-1,1}^2}. \qquad (7)$$

Note that elements in the first column $M_{n,0}$ are always equal to 1.

Equations (5)–(7), which are not present in Ref. 6, allow a more systematic computation of the tridiagonal elements β_n and γ_n. Furthermore, only a few moments were computed in Ref. 6, and none of them applied to the *kagomé* lattice. The much higher-order moments computed here (involving billions of billions of paths), coupled with the systematic evaluation of the parameters β_n and γ_n, give an unprecedented level of accuracy in the derivation of the structure in $T_c(\phi)$.

Below we explicitly express the first few β and γ parameters in terms of the moments; they apply to *any* type of lattice:

$$\beta_1 = 0,$$

$$\beta_2 = \frac{m_3}{z},$$

$$\beta_3 = \frac{m_5 z^2 - 2m_4 m_3 z + m_3^3}{z\alpha},$$

and

$$\gamma_1 = \sqrt{z},$$

$$\gamma_2 = \frac{\sqrt{\alpha}}{z},$$

$$\gamma_3 = \frac{\sqrt{zA}}{\alpha},$$

where

$$\alpha = m_4 z - m_3^2 - z^3$$

and

$$A = m_6 m_4 z - m_6 m_3^2 - m_6 z^3 + 2m_5 m_4 m_3 + 2m_5 m_3 z^2$$
$$- m_5^2 z - 3m_4 m_3^2 z + m_4^2 z^2 - m_4^3 + m_3^4.$$

Using the lattice path integrals obtained, the Hamiltonian matrix elements (β and γ) can be readily computed. For instance, the second-order truncation of the Hamiltonian is

$$H^{(2)} = \begin{pmatrix} 0 & \sqrt{m_2} \\ \sqrt{m_2} & m_3/m_2 \end{pmatrix} = \begin{pmatrix} 0 & 2 \\ 2 & \cos\phi \end{pmatrix}.$$

The presence of the $\cos\phi$ matrix element corresponds (physically) to the Little-Parks oscillations observed in a *single* superconducting loop. Its corresponding top eigenvalue is

$$T_c^{(2)}(\phi) = \frac{1}{2}\left[\frac{m_3}{m_2} + \sqrt{\left(\frac{m_3}{m_2}\right)^2 + 4m_2}\right]$$

$$= \frac{1}{2}\left(\cos\phi + \sqrt{\cos^2\phi + 16}\right).$$

FIG. 3. Superconducting transition temperature, $\Delta T_c^{(n)}(\phi) = T_c(0) - T_c(\phi)$, for a *kagomé* lattice, versus the magnetic flux, ϕ, through an elementary triangular cell, computed from the truncated Hamiltonian. From top to bottom, the orders of truncation are $n = 2$ (top curve), 3, 4, 5, 6, 7, 8, 10, 15, and 19. Note the development of fine structures and cusps. The convergence is monotonic.

The other eigenvalue is not physically important because it does not cross $T_c^{(2)}(\phi)$. $T_c^{(2)}(\phi)$ contains information on the quantum interference effects produced by eight paths (four from m_2 and four from m_3). These closed paths, with at most three steps, cover a very small region of the lattice. The corresponding $\Delta T_c^{(2)}(\phi)$ is the top curve shown in Fig. 3.

The third-order truncation of the Hamiltonian is

$$H^{(3)} = \begin{pmatrix} 0 & \sqrt{m_2} & 0 \\ \sqrt{m_2} & m_3/m_2 & \sqrt{\frac{m_4}{m_2} - \left(\frac{m_3}{m_2}\right)^2 - m_2} \\ 0 & \sqrt{\frac{m_4}{m_2} - \left(\frac{m_3}{m_2}\right)^2 - m_2} & \frac{m_5 m_2^2 - 2m_4 m_3 m_2 + m_3^3}{m_4 m_2^2 - m_3^2 m_2 - m_2^4} \end{pmatrix}$$

$$= \begin{pmatrix} 0 & 2 & 0 \\ 2 & \cos\phi & \sqrt{(5 - \cos 2\phi)/2} \\ 0 & \sqrt{(5 - \cos 2\phi)/2} & \frac{7\cos\phi + \cos 3\phi}{10 - 2\cos 2\phi} \end{pmatrix}.$$

Its corresponding top eigenvalue is

$$T_c^{(3)}(\phi) = \frac{8\cos\phi}{3\lambda} + \frac{31 - 11\cos 2\phi}{3\lambda\Theta^{\frac{1}{3}}} + \frac{32(1 + \cos 2\phi)}{9\lambda^2\Theta^{\frac{1}{3}}} + \Theta^{\frac{1}{3}},$$
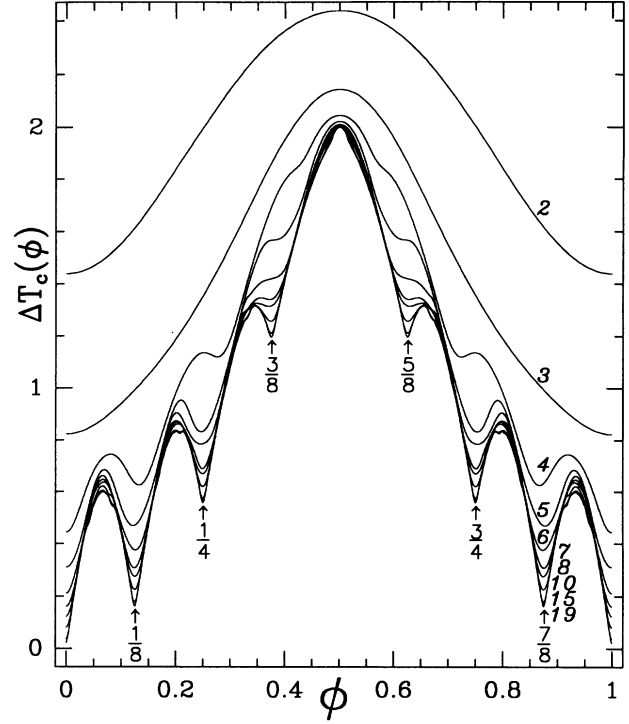
where

$$\lambda = 5 - \cos 2\phi$$

and

$$\Theta = \frac{512 \cos^3 \phi}{27\lambda^3} + \frac{102 \cos \phi - 22 \cos 3\phi}{3\lambda^2} - \frac{7 \cos \phi + \cos 3\phi}{\lambda}$$
$$+ \frac{\sqrt{3}}{9\lambda^2} \left(54 \cos^5 2\phi - 2285 \cos^4 2\phi + 17832 \cos^3 2\phi - 72982 \cos^2 2\phi + 171866 \cos 2\phi - 179509\right)^{\frac{1}{2}}.$$

We have analytically obtained all the eigenvalues of $H^{(3)}$. However, the top one is the only one with physical significance to our problem, because the two other eigenvalues (not shown here) do not cross it. $T_c^{(3)}(\phi)$ contains terms up to 10ϕ, and the corresponding $\Delta T_c^{(3)}(\phi)$ is shown in Fig. 3 (curve labeled by 3). $T_c^{(3)}(\phi)$ exhibits a few terms which follow the Little-Parks $\cos \phi$-type oscillations and also many additional contributions that go well beyond the single-loop effect since they are rigorously derived by summing 96 closed paths on the lattice.

The fourth-order truncation is given by

$$H^{(4)} = \begin{pmatrix} 0 & 2 & 0 & 0 \\ 2 & \cos \phi & \sqrt{(5 - \cos 2\phi)/2} & 0 \\ 0 & \sqrt{(5 - \cos 2\phi)/2} & \frac{7 \cos \phi + \cos 3\phi}{10 - 2 \cos 2\phi} & \gamma_4 \\ 0 & 0 & \gamma_4 & U/V \end{pmatrix},$$

where

$$\gamma_4 = \sqrt{\frac{132 - 64 \cos 2\phi - 6 \cos 4\phi + 20 \cos 6\phi - 2 \cos 8\phi}{51 - 20 \cos 2\phi + \cos 4\phi}},$$

$$U = 344 \cos \phi - 109 \cos 3\phi - 240 \cos 5\phi$$
$$+ 570 \cos 7\phi - 124 \cos 9\phi + 7 \cos 11\phi,$$

and

$$V = 692 - 449 \cos 2\phi - 8 \cos 4\phi$$
$$+ 104 \cos 6\phi - 20 \cos 8\phi + \cos 10\phi.$$

We have also analytically obtained all the eigenvalues of $H^{(4)}$. They exhibit terms which follow the $\cos \phi$-type oscillations and also very many additional contributions which are rigorously derived by summing 1144 closed paths on the lattice.

In general, $T_c^{(n)}(\phi)$ is obtained from the following moments: m_2, m_3, ..., and m_{2n-1}. These contain information on the quantum interference effects due to closed paths of $2n - 1$ steps.

In the following, we physically analyze how the approximations work for the phase diagrams and how the local geometries of the lattices affect the structures in them. Figure 3 shows the second- through eighth-, and also the tenth-, 15th-, and 19th-order approximants to the phase diagram. The fine structures that appear in the lower-order approximants become sharper when the order is increased. Eventually, the dips become cusps. Since the 15th–19th approximants are essentially identical, close convergence to the infinite system size has been achieved. The cusps at $\phi = 1/8$, $1/4$, $3/8$, $5/8$, $3/4$, and $7/8$ are well established in the highest order shown. The resulting phase diagram originates from a competi-

tion between phase coherence at different length scales, which can be explicitly read from the corresponding expressions of the moments.

Quantitatively, there are several differences between the $T_c(\phi)$ for the *kagomé* and, for instance, its perhaps most similar Bravais lattice: the triangular network. The following simple argument illustrates a clear quantitative difference. For the triangular lattice, the energy is minimized when $\phi = n\Phi_0$, where n is an integer, ϕ is the flux through an elementary triangular cell, and Φ_0 is equal to 2π times the quantum of flux. For the *kagomé* case this is also true: When $\phi = \Phi_0$, then $\phi_h = 6\Phi_0$, where ϕ_h is the flux enclosed by an elemental hexagon. However, when $\phi = \Phi_0/6$, the hexagons are in their lowest energy configuration, but the triangles are not. Thus, this particular value of the flux ($\phi = \Phi_0/6$) minimizes the energy of the hexagonal elementary plaquettes in the *kagomé* lattice and *none* of the elementary cells in the triangular lattice. This difference will be reflected in the values for T_c at $\phi = \Phi_0/6$.

Another difference between the phase boundaries of the *kagomé* and other regular lattices (e.g., square, triangular, hexagonal) is that the latter *all* have a prominent minima when the flux per elementary plaquette is equal to $\Phi_0/2$, while the *kagomé* lattice does not.

This concludes our calculation and the main scope of our paper. In the next two sections, we briefly discuss experimental issues and some relations to the magnetic ground state of the XY *kagomé* Hamiltonian.

V. HEISENBERG ANTIFERROMAGNETISM VERSUS SUPERCONDUCTIVITY IN *KAGOMÉ* LATTICES

In superconducting wire networks and arrays of Josephson-coupled islands, the measured $T_c(\phi)$ is often obtained from the maximum (or some other nearby) value of dR/dT, where R is the resistance; i.e., the measured T_c is close, but not necessarily equal, to the real T_c. This measured T_c can be theoretically computed with good accuracy by solving linearized mean-field equations (instead of solving, for instance, the original XY Hamiltonian for the Josephson-coupled islands). The mean field is appropriate because fluctuations are not important as long as the measurements are not extremely close to the real T_c, which is the typical case. Also, by far the dominant effect on any given superconducting island is given by the nearest-neighboring islands, and the mean-field considers an average over them. A better approximation (called a cluster mean field) consists in considering a thermal average over farther neighbors.[6] This procedure incorporates a significant amount of thermal fluc-

tuations. Another approach to incorporate fluctuations uses real-space renormalization-group techniques.[6] Even the simplest mean field for N coupled islands gives N coupled nonlinear complex differential equations which in general are difficult to solve. Linearization simplifies the mathematical treatment of the problem and is also a very physical consideration because the density of Cooper pairs (or order parameter) is small near the transition. Thus, T_c can be conveniently obtained from the ground-state energy of this linearized mean-field model.

After all these steps (i.e., meanfield and linearization), it is not clear that all the information present in the original (XY Hamiltonian) problem can be observed in a narrow part of phase space, i.e., close to the phase boundary. Even if the original information is still there, it is not clear to us that T_c is the best way to access it. For example, the steps in between, from the (initial) full XY Hamiltonian to the (final) linearized mean-field equations, might reduce the symmetry of the problem, and some of the essential information will be lost, or still there but difficult to unmask in a transparent and quantitative way.

The antiferromagnetic XY model on the *kagomé* lattice has a degenerate ground state, and T_c does not seem to reflect this feature because T_c does not contain all the information that can be obtained from the full XY model (or the full nonlinear Ginzburg-Landau equations), but only part of it. Thus, it is not obvious to us how the degeneracy of the ground state of the antiferromagnetic XY model influences T_c.

This paper does *not* focus on degeneracy issues, which are beyond the scope of this work, but on a many-loop version of the Aharonov-Bohm-type argument to derive the origin of the phase boundary features exhibited by superconducting networks. This approach involves moving electrons around loops threaded by a magnetic field, and examining the effect of this electron transport on both the electronic wave functions and ground state energy (T_c).

VI. SUGGESTED EXPERIMENTS ON *KAGOMÉ* SUPERCONDUCTING NETWORKS

A measurement of $\Delta T_c(\phi)$ on a *kagomé* lattice would provide a phase boundary with features which are different from the ones obtained in all the other networks studied so far (e.g., the absence of a prominent minimum at $\Phi_0/2$ and other features discussed in Sec. IV). More importantly, the *kagomé* phase boundary has many sharp dips, unlike, e.g., the relatively dull and featureless phase diagram for the hexagonal network. It appears to us that the dips (cusps) in the *kagomé* $\Delta T_c(\phi)$ are the *sharpest* of all regular lattices. These sharp dips are predicted[6] to become even sharper when the measurements are made closer to the real T_c. Furthermore, the current state of the technology would allow the construction of lattices which are far more perfect than the ones previously built. Thus, a direct comparison between measurements and our Fig. 3 could be made.

The Heisenberg and the XY *kagomé* antiferromag-

nets have attracted considerable attention for the reasons mentioned in our opening paragraph and discussed in detail in Refs. 1–3. These models exhibit geometrical frustration which prevents the establishment of long-range magnetic order. The classical Hamiltonians exhibit a complicated ground-state degeneracy, with both non-coplanar and planar states in the degenerate manifold.

In order to look for possible manifestations of the degeneracy and extensive entropy of the antiferromagnetic XY ground state, experiments could perhaps focus also away from T_c. At lower temperatures, the imaging of the vortex lattice could provide a picture of the XY spin state, because the phases of the order parameters would be arranged as the XY spin configuration of a *kagomé* antiferromagnet. At lower temperatures, the nonlinearity (e.g., quartic term in the Ginzburg-Landau free energy) breaks the degeneracy present in the linear approximation. When lowering the temperature, the density of Cooper pairs increases and it is not possible to linearize the equations. Thus, the full Hamiltonian must be used.

The variation of the phases (of the order parameter) between nearby islands will produce loop currents and their associated fields could, in principle, be measured using a variety of different probes like (a) a scanning tunneling microscope, (b) a scanning atomic force microscope, (c) a scanning Hall probe, and/or (d) inductive measurements like the ones employed by Martinoli's group.[4] Thus, information on the currents and/or flux configurations would be helpful to determine the phase arrangement (XY spins on a *kagomé* lattice).

VII. DISCUSSIONS

The iterative approach presented above can be thought of as an analytical version of a hybrid between modified Lanczos and moments methods, both typically used in purely numerical procedures. It not only provides us with a systematic approximation scheme for the phase diagrams, but also a rather powerful tool for a qualitative and quantitative analysis of the structures in them and their physical origin. As the order of approximation is increased, more geometrical information of the lattice is included in the interference treatment, and more fine structures are resolved. The correspondence is such that we can draw a number of specific conclusions regarding how the dips of various sizes in $T_c(B)$ are related to the geometry of the underlying lattice. The gross structure is determined by the interference effects arising from few loops. The secondary dips or peaks are determined by the additional information provided by interference arising from higher-order lattice path integrals (i.e., larger paths that explore more loops). In general, higher-order fine structures are due to interference among the cells of larger clusters (here including as many as 10^{21} loops). The indexing of the dips ($\phi = n/8$, where $n = 1, 2, 3, 5, 6, 7$) in the phase diagrams can be easily read off from the periods of the truncated matrix elements. The sharpness of the dips is due to *long-range* correlations, and cannot be accounted for by local geometries. We expect our predictions to compare well with future experiments on this system.

ACKNOWLEDGMENTS

APPENDIX: LATTICE PATH INTEGRALS M_{16}–M_{20}

$m_{16} = 41001292 + 25428480\cos 2\phi + 918560\cos 4\phi + 9092352\cos 6\phi + 15316256\cos 8\phi + 2863616\cos 10\phi$
$\qquad +109088\cos 12\phi + 890560\cos 14\phi + 956304\cos 16\phi + 112000\cos 18\phi + 5120\cos 20\phi + 53568\cos 22\phi$
$\qquad +42912\cos 24\phi + 2688\cos 26\phi + 192\cos 28\phi + 2752\cos 30\phi + 1440\cos 32\phi + 64\cos 38\phi\,,$

$m_{17} = 218660460\cos\phi + 23053020\cos 3\phi + 11763116\cos 5\phi + 61614120\cos 7\phi + 36265760\cos 9\phi + 2637380\cos 11\phi$
$\qquad +1726928\cos 13\phi + 5807812\cos 15\phi + 2339200\cos 17\phi + 113832\cos 19\phi + 135388\cos 21\phi + 385492\cos 23\phi$
$\qquad +112200\cos 25\phi + 2992\cos 27\phi + 9180\cos 29\phi + 23052\cos 31\phi + 4080\cos 33\phi + 340\cos 37\phi + 748\cos 39\phi\,,$

$m_{18} = 504967204 + 358082904\cos 2\phi + 21570528\cos 4\phi + 143901532\cos 6\phi + 240951024\cos 8\phi + 56411064\cos 10\phi$
$\qquad +3381816\cos 12\phi + 19345860\cos 14\phi + 22651848\cos 16\phi + 3827416\cos 18\phi + 256560\cos 20\phi + 1688400\cos 22\phi$
$\qquad +1610136\cos 24\phi + 195084\cos 26\phi + 17064\cos 28\phi + 136752\cos 30\phi + 105120\cos 32\phi + 7560\cos 34\phi$
$\qquad +720\cos 36\phi + 7668\cos 38\phi + 168\cos 46\phi + 12\cos 54\phi\,,$

$m_{19} = 2799941004\cos\phi + 382148520\cos 3\phi + 208697444\cos 5\phi + 932000464\cos 7\phi + 603749320\cos 9\phi$
$\qquad +60413692\cos 11\phi + 38512392\cos 13\phi + 120342732\cos 15\phi + 57911316\cos 17\phi + 4436880\cos 19\phi$
$\qquad +4161456\cos 21\phi + 11250660\cos 23\phi + 4359132\cos 25\phi + 246088\cos 27\phi + 408804\cos 29\phi$
$\qquad +1005176\cos 31\phi + 303240\cos 33\phi + 10336\cos 35\phi + 30172\cos 37\phi + 67108\cos 39\phi$
$\qquad +12540\cos 41\phi + 1064\cos 45\phi + 2128\cos 47\phi + 76\cos 53\phi + 152\cos 55\phi\,,$

$m_{20} = 6338429028 + 4999672400\cos 2\phi + 445104760\cos 4\phi + 2233225680\cos 6\phi + 3683951360\cos 8\phi$
$\qquad +1025139280\cos 10\phi + 87649740\cos 12\phi + 383654240\cos 14\phi + 471275520\cos 16\phi + 102042960\cos 18\phi$
$\qquad +9360020\cos 20\phi + 44470640\cos 22\phi + 46514880\cos 24\phi + 8109600\cos 26\phi + 883500\cos 28\phi + 4886400\cos 30\phi$
$\qquad +4442160\cos 32\phi + 595120\cos 34\phi + 69960\cos 36\phi + 438800\cos 38\phi + 328240\cos 40\phi + 26400\cos 42\phi$
$\qquad +2800\cos 44\phi + 24080\cos 46\phi + 12320\cos 48\phi + 200\cos 52\phi + 2080\cos 54\phi + 880\cos 56\phi + 80\cos 62\phi\,.$

[1] P. Chandra, P. Coleman, and I. Ritchey, J. Phys. (Paris) 3, 591 (1993); P. Chandra and P. Coleman, Les Houches Lectures (in press); Phys. Rev. Lett. 66, 100 (1991); A. Chubukov, ibid. 69, 832 (1992); E. F. Shender, V. B. Cherepanov, P. C. W. Holdsworth, and A. J. Berlinsky, ibid. 70, 3812 (1993); K. Yang, L. K. Warman, and S. M. Girvin, ibid. 70, 2641 (1993); C. Zeng and V. Elser, Phys. Rev. B 42, 8436 (1990); P. W. Leung and V. Elser, ibid. 47, 5459 (1993); A. B. Harris, C. Kallin, and A. J. Berlinsky, ibid. 45, 2899 (1992); T. C. Hsu and A. J. Schofield, J. Phys. Condens. Matter 3, 8067 (1991).

[2] V. Elser, Phys. Rev. Lett. 62, 2405 (1989); D. S. Greywall and P. A. Busch, ibid. 62, 1868 (1989); 65, 2788 (1990).

[3] A. P. Ramirez, G. P. Espinoza, and A. S. Cooper, Phys. Rev.

Lett. 64, 2070 (1990); C. Broholm, G. Aepli, G. P. Espinosa, and A. S. Cooper, ibid. 65, 3173 (1990); I. Ritchey, P. Coleman, and P. Chandra, Phys. Rev. B 47, 15342 (1993).

[4] See, for instance, the reviews by B. Pannetier, J. Chaussy, and R. Rammal, Jpn. J. Appl. Phys. 26, Suppl. 26-3, 1994 (1987); P. Martinoli, ibid. 26, Suppl. 26-3, 1989 (1987); C. J. Lobb, Physica 126B, 319 (1984); and the many articles in the issue on "Coherence in superconducting networks," edited by J. E. Mooij and G. B. J. Schön [Physica 152B, 1 (1988)].

[5] J. von Delft and C. L. Henley, Phys. Rev. Lett. 69, 3236 (1992).

[6] Q. Niu and F. Nori, Phys. Rev. B 39, 2134 (1989).

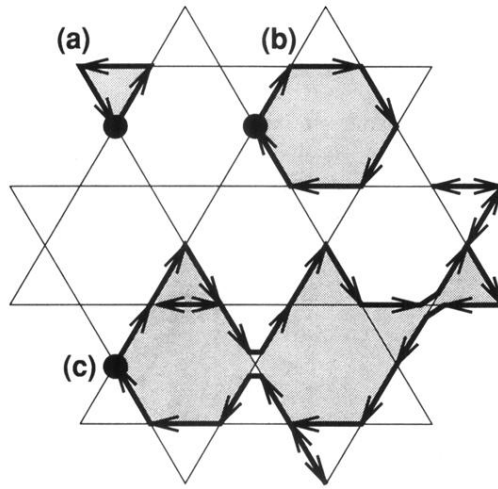[7] W. Y. Shih and D. Stroud, Phys. Rev. B 32, 158 (1985).

FIG. 1. Several examples of closed paths on a *kagomé* lattice and their respective phase factor contributions to the lattice path integrals. (a) Traversing counterclockwise a three-step path on an elementary triangular cell contributes a term $e^{i\phi}$ to m_3, (b) a six-step clockwise walk on an elementary hexagonal loop contributes a term $e^{-6i\phi}$ to m_6, and (c) a closed path of 26 steps with several links retraced. Its phase factor is $e^{-16i\phi}$. The solid dots denote the starting (and ending) sites and the arrows specify the hopping directions on bonds.